Winter Wonderland Cave, Utah, USA: A Natural Laboratory for the Study of Cryogenic Cave Carbonate and Thawing Permafrost

Jeffrey Munroe (jmunroe@middlebury.edu)
Middlebury College
Kristin Kimble
Middlebury College
Christoph Spötl
Universität Innsbruck
Gabriela Serrato Marks
Massachusetts Institute of Technology
David McGee
Massachusetts Institute of Technology
David Herron
US Forest Service

Research Article

Keywords: CCC, cryogenic, Holocene

Posted Date: December 4th, 2020

DOI: https://doi.org/10.21203/rs.3.rs-114446/v1

Version of Record: A version of this preprint was published at Scientific Reports on March 19th, 2021. See the published version at https://doi.org/10.1038/s41598-021-85658-9.

Abstract

Winter Wonderland Cave contains perennial ice associated with two types of cryogenic cave carbonate (CCC) formed during the freezing of water. CCC_{fine} is characterized by relatively enriched $\delta^{13}C$ values, whereas CCC_{coarse} exhibits notably depleted $\delta^{18}O$ values indicating precipitation under (semi)closed-system conditions in a pool of residual water beneath an ice lid. Previous work has concluded that CCC_{coarse} forms during permafrost thaw, making the presence of this precipitate a valuable indicator of past cryospheric change. Available geochronologic evidence indicates that CCC formation in this cave is a Late Holocene or contemporary process, and field observations suggest that the cave thermal regime recently changed in a manner that permits the ingress of liquid water. This is the first documented occurence of CCC_{coarse} in the Western Hemisphere and one of only a few locations where these minerals have been found in association with ice. Winter Wonderland Cave is a natural laboratory for studying CCC genesis.

Introduction

The cryosphere is responding rapidly to climate warming, and paleoclimate records are critical for understanding the novelty of these responses[1,2]. A persistent challenge is that many paleoclimate archives are biased toward extremes, for instance the most extensive glacial advances[3], most widespread periglacial conditions[4], or sea level high- and low-stands[5]. Yet records of past climatic transition are crucial for placing contemporary global change into a longer-term context[6]. This is especially true in Arctic and high mountain environments where temperatures are warming rapidly[7,8], leading to dramatic diminishment of ice extent[9,10] and degradation of permafrost[11,12]. Thus there is an urgent need for better records of how the cryosphere changed in the past, to clarify when and how rapidly changes occurred, and in what pattern these changes unfolded across the landscape.

A unique proxy demonstrated to provide information about past episodes of permafrost thaw, a transition that is often particularly disruptive to landscapes, ecosystems and infrastructure, is cryogenic cave carbonate (CCC). These minerals form when liquid water enters a cave containing subzero temperature conditions[13]. As this water freezes, solutes are concentrated in the remaining liquid until saturation is reached and precipitation of CCC is induced[14,15]. Although seasonal subzero conditions can be created inside a cave entrance by winter cold, more significant permanently subzero conditions are maintained in so-called “ice caves” by ventilation regimes that preferentially allow the ingress of winter air while excluding summer warmth[16,17]. For instance, caves with a single downward sloping entrance can trap cold air through density settling in winter; air that is not replaced by warmer, less dense air in the summer. Alternatively, caves with multiple entrances at different elevations are susceptible to chimney effects that support freezing conditions where large amounts of cold air are pulled into the cave in winter. Either way, CCC is precipitated when water containing sufficient dissolved solutes encounters the subzero conditions.

Two types of CCC have been identified. One group, referred to as CCC_{fine}, forms when a film of water freezes on the surface of pre-existing ice[18]. The large surface area of this thin layer facilitates degassing of CO_2, preferentially removing ^{12}C, and leaving the remaining water enriched in ^{13}C through kinetic effects[19,20]. Simultaneously, the preferential incorporation of ^{18}O in the ice is counterbalanced by evaporation of lighter $H_2{}^{16}O$ from the water surface, yielding a characteristically enriched $\delta^{13}C$ and relatively unaltered $\delta^{18}O$ signature[18]. The ice involved in the formation of CCC_{fine} does not need to be perennial, however the presence of CCC_{fine} in a currently ice-free cave is nonetheless clear evidence for colder conditions in the past.

In contrast, CCC_{coarse} is a more specific proxy because it forms when a descending permafrost table driven by permafrost thaw intersects the upper part of a cave, allowing dripwater to enter and form pools on the ice surface[21,22]. Because the temperature in the main part of the cave (below the permafrost table) is still subzero, these pools freeze over, creating (semi)closed-system conditions in which degassing of CO_2 and evaporation of water are greatly reduced[21]. Slow freezing of these isolated volumes of water precipitates CCC_{coarse} distinguished by less enriched $\delta^{13}C$ and notably depleted values of $\delta^{18}O$ compared with CCC_{fine}[13,15,23]. As is apparent throughout Arctic and high mountain environments today, elevation of ground temperature above 0°C, thawing of permafrost, and melting of ground ice are step-changes with dramatic repercussions for landscape and environmental evolution[24]. CCC_{coarse}, therefore, is a critical proxy because it records past episodes of permafrost thaw.

Here we report the first discovery of CCC_{coarse} in North America from an unusual setting where apparently young CCC is present in association with modern perennial ice. Our work provides an important point of comparison for CCC from well-studied caves in Europe, and documents a setting in which theories for CCC genesis could be evaluated.

Location

The CCC studied in this project was collected from Winter Wonderland Cave (WWC) in the Uinta Mountains of northeastern Utah, USA (Fig. 1). This solution cave has developed in the Carboniferous-age Madison Limestone, a regionally extensive rock unit that in this area consists of fine to coarse-grained dolomite and limestone, with locally abundant nodules of chert[25]. The entrance to WWC is at an elevation of 3140 m asl in a north-facing cliff at the edge of the karstified Blind Stream Plateau (40.53°N, 110.73°W), a sparsely forested subalpine landscape. The mean annual air temperature (1985-2020) at the Brown Duck snowpack telemetry (SNOTEL) station at a similar elevation (3223 m) 12 km to the east of WWC is 0.3°C (https://wcc.sc.egov.usda.gov/nwcc/site?sitenum=368). Elsewhere in the Uinta Mountains, the Chepeta remote automated weather station (RAWS) at an elevation of 3694 m recorded a mean temperature of -2.0°C between 2000 and 2019 (https://wrcc.dri.edu/cgi-bin/rawMAIN.pl?utCHEP). Inside WWC temperatures were consistently subzero from 2016-2018 because of a ventilation regime that brings cold winter air in through the main entrance, and inhibits the entry of warm air in the summer. As a result, about half of the cave, which has a mapped length of 245 m, is floored by perennial ice up to 3 m thick. CCC is present as a lag on the ice surface, drapes rocks emerging from the sublimating ice, and occurs as discrete layers within the ice body (Fig. 2a). Additional details about the cave and its climatology are presented in Munroe (2020).

Representative CCC samples, numbered YS-1 through YS-6 (Table S1) were collected from the ice surface along with three samples that were submerged in small (~10-30 cm deep) pools (Fig. 2b) of water filling depressions in the ice (CP, YP, and TF). Additional samples of Madison Limestone bedrock and water from pools were also collected for analysis.

Results And Interpretation

CCC Morphology.

An array of morphologies is present in the CCC samples from WWC. The smallest size fractions are spherulitic, with large aggregates reaching diameters of 50 μm, and individual spherules from 10 to 20 μm in diameter (Fig. 2c). This observation is corroborated by results from laser scattering, which reveal mean grain sizes from 24 to 42 μm in the <75-μm fraction. Rounded grains are typically clumped in botryoidal aggregates with smooth surfaces, and dumbbell structures are common. Occasionally more sharp-edged morphologies are present, with needle-like points that rarely exceed 5 μm in length. Larger size fractions (250-75 μm) contain rafts of aggregated grains in excess of 200 μm long. The TF samples, which were collected from the water surface, are characterized by arrow-shaped blades 10 to 20 μm long, grouped into thin rafts (Fig. 2d). All of these observations match CCC morphologies reported in the literature. For instance, previous work has established that CCC often occurs as raft-like aggregates of crystals, and spherical forms[21,22,26]. Rafts are generally flat and composed of interlocking crystals in a manner similar to floating carbonate minerals reported from non-cryogenic cave environments[27]. Crystal splitting has been invoked as a mechanism for the growth of spherical forms[28], which are sometimes superimposed on a branching, sheaf-life skeleton[29]. Finally, spherules are reported to display smooth surfaces, and often connect during growth to form dumbbell shapes[21] or chains[22].

On the other hand, the CCC in WWC is considerably finer than precipitates with similarly depleted $\delta^{18}O$ values reported from European caves. Although there is a wide range in sizes, CCC is typically described as having crystals from <1 mm to ~40 mm[21,22,26] compared with the 10 to 20-μm diameter spherules common in WWC. The significance of this difference is unclear; it may simply indicate that CCC in WWC formed from smaller-volume pools, or from water with a lower total dissolved load.

Types of CCC Present in WWC. Although, as their names suggest, early studies differentiated CCC_{fine} and CCC_{coarse} by grain size, $\delta^{13}C$ and $\delta^{18}O$ data reflecting different C and O isotope fractionation mechanisms are now recognized as the only valid criteria for distinguishing between the two groups[18]. With this in mind, values of $\delta^{13}C$ and $\delta^{18}O$ indicate that both types of CCC are present in WWC (Fig. 3a).

Samples YS-3 and YS-4 have $\delta^{13}C$ averaging 6‰ and an average $\delta^{18}O$ of -7.3‰ (Table S2), suggesting that both are CCC_{fine}. In contrast, samples YS-1, YS-2, YS-5, YS-6, CP, and YP have lower values of $\delta^{13}C$, averaging 3.5‰, and notably more depleted $\delta^{18}O$, averaging -16‰. These values identify these samples as CCC_{coarse} (Table S2). Sample TF also plots in the CCC_{coarse} field (Fig. 3a), although it was collected from a pool that had just begun to freeze, which may explain why its $\delta^{18}O$ value is less depleted than the other CCC_{coarse} samples. For comparison, samples of the Madison Limestone collected in WWC have an average $\delta^{13}C$ of 2.2‰ and $\delta^{18}O$ of -5.9‰ (Fig. 3a). Consistency of stable isotope values within individual size fractions (250-165 μm, 165-75 μm, and <75 μm) emphasizes that YS-5, YS-6, CP, and YP are pure CCC_{coarse} (Fig. 3b). In YS-1 and YS-2, CCC_{coarse} is concentrated in the <75-μm fraction. In contrast, YS-4 is consistently CCC_{fine} in all size fractions.

The results of additional analyses permit further interpretation of these samples. XRD reveals that YS-3 and YS-4 (CCC_{fine}) are a mixture of calcite and quartz (Fig. S1), and rounded quartz grains were visible in the <250-μm size fraction. The presence of quartz is confirmed in the XRF results, where sample YS-4 contains 52% SiO_2 (Table S3). YS-3 and YS-4 also have much higher chondrite-normalized REE values (Table S4, Fig. S2). These observations, along with the isotope data for size fractions presented above, are evidence for a detrital component in these CCC_{fine} samples, which were collected from bedrock shelves above the current ice surface (Fig. 1). In contrast, XRD analysis indicates that the CCC_{coarse} samples are composed solely of calcite, as are the bedrock samples (Fig. S1). Major element analysis (Table S3) reinforces the abundance of calcite in YS-6 (70% as CaO), and Mg is considerably more abundant in YS-6 (12.2% as MgO) than in YS-4 (1.8%). Collectively the mineralogical and geochemical analyses support the conclusion from the isotope results that both CCC_{coarse} and CCC_{fine} are present in WWC.

CCC Ages. Previous studies have successfully applied $^{230}Th/^{234}U$ disequilibrium dating[26] to CCC[15]. Accordingly, an attempt was made to date CCC_{coarse} from WWC (Table S5). The resulting ages are imprecise due to low $^{230}Th/^{232}Th$ ratios, a situation that has complicated other work[22,26], meaning that the correction for detrital ^{230}Th, and the uncertainty on that correction, are large. On the other hand, one of the samples analyzed (TF) is clearly modern because it was collected in 2018 from a pool of water that was not present in 2016. The initial $^{230}Th/^{232}Th$ for this sample was, therefore, applied to the others (with a 25% 2-σ uncertainty) to refine the age calculations. Results indicate that the CCC in WWC likely formed during the Holocene, and nearly all of the ages have error estimates that overlap with modern (Table S5, Fig. S3). Thus these ages, imprecise as they are, are consistent with CCC formation as a recent or current process in WWC. This result is significant because the majority of published CCC ages are from the Late Pleistocene[e.g. 21,30], with only a few reports of Holocene ages[22,26,31].

Two additional lines of evidence support the interpretation that the CCC in WWC is young. First, rafts of calcite from sample YS-6 yielded a radiocarbon result of f_{Modern} 1.111 ± 0.005, consistent with formation in the late 20th Century when calibrated with the NH1 bomb curve in Oxcal 4.4[32] (Fig. S4). Second, samples of rodent fecal pellets from the ice beneath the surface lag of CCC yielded radiocarbon ages that calibrate to between AD 1600 and 1850[33] using the IntCal20 calibration curve[34]. Together this evidence strongly supports the conclusion that CCC formation in WWC occurred in the late Holocene, and is still occurring today.

Winter Wonderland Cave as a Unique Natural Laboratory for the study of CCC.

Because of its utility as a paleoclimate proxy, numerous studies have investigated CCC[e.g. 21,30,35,36]. However, there are only a few reports of CCC from locations outside Eurasia[19,37], and all of these are categorized isotopically as CCC_{fine}. Winter Wonderland Cave is, therefore, the first location in the Western Hemisphere where the unique paleoclimate indicator CCC_{coarse} has been identified.

Furthermore, nearly all previous observations of CCC describe these minerals from locations where they are present as loose concentrations of mineral grains on an ice-free cave floor[21,26]. Only twice has CCC_{coarse} been reported in association with modern, perennial ice[31,36], and a recent comprehensive review noted that *"Despite increasing evidence for Holocene CCC_{coarse}, actively forming sites have not yet been observed"*[13]. In WWC, CCC_{coarse} with late Holocene to modern ages is present in association with perennial ice, making this cave an exceptional natural laboratory in which to study these precipitates and their genesis.

Furthermore, firsthand observations indicate that the situation within WWC is consistent with the model for the formation of CCC_{coarse}. During summer visits in 2014, 2015, and 2016, the cave was dry and the ice surface exhibited a complex pattern of elongated ridges and troughs with local relief on the order of 30 cm (Fig. 4) formed as a result of sublimation[38]. Short-term studies in an ice cave in Alberta, Canada suggest ice sublimation rates on the order of 3 mm per year[39], although rates up to 10× higher have also been reported[13]. Either way, extrapolation from these benchmarks suggests that the relief observed on the ice surface in 2016 reflects 10^1 to 10^2 years of sublimation without the addition of new water. In contrast, in summer 2018, and again in 2019, liquid water entered the cave, filling many of the furrows, and freezing to create a new ice surface (Fig. 4). Deeper pools of water had lids of ice from 1 to 5 cm thick (Fig. 2b), precisely the mechanism proposed for the formation of CCC_{coarse}[15,21,23]. This water ranged from clear to a deep yellow color, and CCC was observed on the floor of each pool (Table S1). From the available data we cannot determine if this CCC precipitated from the water, or whether it was present as a lag on the ice surface before the pools formed. However, the concentration of solutes in this pool water was very high, with the highest values (K, Mg, and Ca >200 mg/L) corresponding to the yellow color (Fig. S5), consistent with conditions necessary for mineral precipitation through freezing-induced saturation[14].

The change from 2016 to 2018 suggests that the thermal state of the epikarst has recently shifted, at least locally, to allow liquid water to penetrate to the level of the cave (~100 m below the ground surface), or to produce meltwater from ice farther back in inaccessible parts of the cave system. Under extensive permafrost conditions, caves are unlikely to contain ice sourced from dripwater because the permafrost inhibits the downward movement of liquid water[40]. Only when permafrost is degrading is it possible for liquid water to reach a cave where temperatures remain consistently subzero. The available evidence supports the interpretation that WWC and its surrounding host rock comprise a sporadic permafrost body that is currently undergoing this transition. Numerical modeling suggests that the time window between thawing and ultimate loss of permafrost is relatively short[41], and studies have noted that cave ice is rapidly ablating in various locations around the world[42]. Future investigations in WWC should take advantage of this singular opportunity to observe the formation of different types of CCC in (near) real time, with the goal of improving our ability to use the presence of these features in currently ice-free caves as a dateable indicator of past permafrost thaw[21].

Conclusion

Winter Wonderland Cave in the Uinta Mountains of Utah contains cryogenic cave carbonate (CCC) associated with perennial ice. Two types of CCC with different genesis are present and can be distinguished on the basis of O and C isotope values. CCC_{fine} is produced through open system freezing as a thin film of water flows over the ice surface. In contrast, CCC_{coarse} is produced by (semi) closed-system freezing in deeper pools of water beneath thickening lids of ice. These conditions arise during permafrost thaw, thus CCC_{coarse} records past episodes of permafrost degradation. Available age control suggests that CCC formation occurred in this cave during the late Holocene and may be a contemporary process. This cave is the first location in the world where such young CCC_{coarse} has been found, and is the first location in the Western Hemisphere where CCC_{coarse} has been identified. Records of past cryosphere transitions are critical context for assessing contemporary changes in Arctic and alpine environments. Winter Wonderland Cave provides a singular opportunity to test and improve theories of CCC genesis that will ultimately allow better insight into how permafrost responded to past climatic transitions.

Methods

The methods employed in sample analysis are briefly described here; full details are presented in the supporting information. At Middlebury College, CCC samples were wet sieved into >250, 250-75, and <75 µm size fractions. The morphology of all fractions was examined with a Tescan Vega 3 LMU scanning electron microscope (SEM). Energy dispersive x-ray spectroscopy (EDS) was used to evaluate whether contrasting grain morphologies observed in samples YS-3, YS-6, TS-2, CP, YP, and TF correspond to different elemental compositions.

The grain size distribution of the <75-µm fraction of each sample was investigated with laser scattering in a Horiba LA-950 particle size analyzer. Samples were dispersed in distilled water, and sonified before analysis.

CCC mineralogy, along with representative samples of the Madison Limestone collected from the cave, was investigated with a Bruker D8 Advance x-ray diffractometer. The mineralogy of several samples was compared across different size fractions (<75 μm and 250-75 μm) to detect any compositional differences. Because none were apparent, the <75-μm and 250-75-μm fractions were used interchangeably for subsequent analyses depending on the amount of sample remaining.

The abundance of major elements (Si, Ti, Al, Fe, Mn, Mg, Ca, Na, K, P) in the samples was investigated with x-ray fluorescence on a Thermo Scientific ARL QuantX energy dispersive XRF. Trace elements were measured in the <75-μm fraction of samples YS-3, YS-4, YS-5, YS-6, TS-1, TS-2, in a representative bedrock sample, and in the 250-75-μm fraction of sample YS-4 with inductively coupled plasma mass spectrometry on a Thermo Scientific iCAP Q ICP-MS after dissolution in HNO_3. The ICP-MS was also used to investigate the hydrochemistry of the water samples.

Values of $\delta^{18}O$ and $\delta^{13}C$ were measured in all <75-μm size fractions except CP and YP 250-75 μm at Union College using a GasBench II connected to a Thermo Delta Advantage isotope ratio mass spectrometer in continuous flow mode. Analytical uncertainties were better than 0.1 ‰ (1σ) for $\delta^{18}O$ and 0.05 ‰ (1σ) for $\delta^{13}C$. Eleven samples of bedrock, along with separate size fractions of samples YS-1 through YS-6, CP, and YP were analyzed at the University of Innsbruck on a Thermo Scientific Delta V Plus isotope ratio mass spectrometer (IRMS) connected to a GasBench II[43]. This system produces a typical precision (1σ) of ±0.06 ‰ for $\delta^{13}C$ and ±0.08 ‰ for $\delta^{18}O$[44]. All isotope results were calibrated against international standards and reported in permil (‰) relative to VPDB.

The age of 5 samples (YS-5, YS-6, CP, YP, and TF) was assessed using U-Th techniques at the Massachusetts Institute of Technology. U and Th were analyzed on separate aliquots using a Nu Plasma II-ES multi-collector ICP-MS equipped with a CETAC Aridus II desolvating nebulizer[45]. U-Th ages were first calculated using standard decay constants for ^{230}Th, ^{234}U, and ^{238}U[46–48], then recalculated given the observation that the TF sample is modern. Reported errors for ^{238}U and ^{232}Th concentrations are estimated to be ±1% due to uncertainties in spike concentration, whereas analytical errors are smaller. Variability of initial $^{230}Th/^{232}Th$ throughout the cave was assumed to be ±25% at 2σ.

Declarations

Data Availability: The dataset generated in this study has been deposited in the Hydroshare repository and will have the doi https://doi.org/10.4211/hs.b5f0000096174af9af94fe62bd2065d6 *after publication*.

Acknowledgments

C.W. was crucial to the success of this challenging fieldwork. P.R. and J.S. assisted with the ICP-MS analysis. Thanks to D.G. at Union College for help with the initial isotope measurements. Financial support was provided by the Middlebury College URO.

Author Contributions:

JM designed the study, wrote the manuscript, and prepared the figures. KK participated in fieldwork, conducted the geochemical and preliminary isotope analyses, and prepared samples for U/Th dating. CS oversaw isotope analyses at the University of Innsbruck. DM and GSM oversaw the U/Th dating at MIT. DH ensured safe passage to and from the cave, and provided the mapping upon which Figure 1 was based. All authors reviewed the manuscript before submission.

Competing Interests: The authors declare no conflict of interest.

References

1. Adler, C., Huggel, C., Orlove, B. & Nolin, A. Climate change in the mountain cryosphere: impacts and responses. *Regional Environmental Change* **19**, 1225–1228 (2019).
2. Overland, J. *et al.* The urgency of Arctic change. *Polar Science* **21**, 6–13 (2019).
3. Mackintosh, A. N., Anderson, B. M. & Pierrehumbert, R. T. Reconstructing Climate from Glaciers. *Annu. Rev. Earth Planet. Sci.* **45**, 649–680 (2017).
4. Lindgren, A., Hugelius, G., Kuhry, P., Christensen, T. R. & Vandenberghe, J. Gis-based maps and area estimates of northern hemisphere permafrost extent during the last glacial maximum. *Permafrost and Periglacial Processes* **27**, 6–16 (2016).
5. Murray-Wallace, C. V. & Woodroffe, C. D. *Quaternary sea-level changes: a global perspective*. (Cambridge University Press, 2014).
6. Maslin, M., Seidov, D. & Lowe, J. Synthesis of the nature and causes of rapid climate transitions during the quaternary. *Washington DC American Geophysical Union Geophysical Monograph Series* **126**, 9–52 (2001).
7. Palazzi, E., Mortarini, L., Terzago, S. & Von Hardenberg, J. Elevation-dependent warming in global climate model simulations at high spatial resolution. *Climate Dynamics* **52**, 2685–2702 (2019).
8. Zhang, J. Warming of the arctic ice-ocean system is faster than the global average since the 1960s. *Geophysical Research Letters* **32**, (2005).
9. Meier, W. N. *et al.* Arctic sea ice in transformation: A review of recent observed changes and impacts on biology and human activity. *Reviews of Geophysics* **52**, 185–217 (2014).
10. Sommer, C. *et al.* Rapid glacier retreat and downwasting throughout the European Alps in the early 21 st century. *Nature communications* **11**, 1–10 (2020).
11. Marcer, M. *et al.* Inferring the destabilization susceptibility of mountain permafrost in the French Alps using an inventory of destabilized rock glaciers. *The Cryosphere Discussions* 1–30 (2018).
12. Rudy, A. C. A., Lamoureux, S. F., Kokelj, S. V., Smith, I. R. & England, J. H. Accelerating thermokarst transforms ice-cored terrain triggering a downstream cascade to the ocean. *Geophysical Research Letters* **44**, 11–080 (2017).
13. Žák, K. *et al.* Cryogenic mineral formation in caves. in *Ice caves* 123–162 (Elsevier, 2018).

14. Killawee, J. A., Fairchild, I. J., Tison, J.-L., Janssens, L. & Lorrain, R. Segregation of solutes and gases in experimental freezing of dilute solutions: Implications for natural glacial systems. *Geochimica et Cosmochimica Acta***62**, 3637–3655 (1998).
15. Žák, K., Urban, J., Cılek, V. & Hercman, H. Cryogenic cave calcite from several Central European caves: age, carbon and oxygen isotopes and a genetic model. *Chemical Geology***206**, 119–136 (2004).
16. Luetscher, M. & Jeannin, P.-Y. The role of winter air circulations for the presence of subsurface ice accumulations: an example from Monlési ice cave (Switzerland). *Theoretical and Applied Karstology***17**, (2004).
17. Luetscher, M. & Jeannin, P.-Y. A process-based classification of alpine ice caves. *Theoretical and Applied Karstology***17**, 5–10 (2004).
18. Žák, K., Onac, B. P. & Perşoiu, A. Cryogenic carbonates in cave environments: A review. *Quaternary International***187**, 84–96 (2008).
19. Clark, I. D. & Lauriol, B. Kinetic enrichment of stable isotopes in cryogenic calcites. *Chemical Geology***102**, 217–228 (1992).
20. Lacelle, D., Lauriol, B. & Clark, I. D. Effect of chemical composition of water on the oxygen-18 and carbon-13 signature preserved in cryogenic carbonates, Arctic Canada: implications in paleoclimatic studies. *Chemical Geology***234**, 1–16 (2006).
21. Žák, K. *et al.* Coarsely crystalline cryogenic cave carbonate-a new archive to estimate the Last Glacial minimum permafrost depth in Central Europe. *Climate of the Past***8**, (2012).
22. Luetscher, M., Borreguero, M., Moseley, G. E., Spötl, C. & Edwards, R. L. Alpine permafrost thawing during the Medieval Warm Period identified from cryogenic cave carbonates. *Cryosphere***7**, 1073–1081 (2013).
23. Richter, D. K., Meissner, P., Immenhauser, A., Schulte, U. & Dorsten, I. Cryogenic and non-cryogenic pool calcites indicating permafrost and non-permafrost periods: a case study from the Herbstlabyrinth-Advent Cave system (Germany). *The Cryosphere***4**, 501 (2010).
24. Oliva, M. & Fritz, M. Permafrost degradation on a warmer Earth: Challenges and perspectives. *Current Opinion in Environmental Science & Health***5**, 14–18 (2018).
25. Bryant, B. *Geologic and structure maps of the Salt Lake City 1 x 2 quadrangle, Utah and Wyoming*. (US Geological Survey, 1992).
26. Spötl, C. & Cheng, H. Holocene climate change, permafrost and cryogenic carbonate formation: insights from a recently deglaciated, high-elevation cave in the Austrian Alps. *Climate of the Past***10**, 1349–1362 (2014).
27. Jones, B. Calcite rafts, peloids, and micrite in cave deposits from Cayman Brae, British West Indies. *Can. J. Earth Sci.***26**, 654–664 (1989).
28. Meakin, P. & Jamtveit, B. Geological pattern formation by growth and dissolution in aqueous systems. *Proceedings of the Royal Society A: Mathematical, Physical and Engineering Sciences***466**, 659–694 (2010).

29. Chaykovskiy, I. I., Kadebskaya, O. I. & ák, K. Morphology, composition, age and origin of carbonate spherulites from caves of Western Urals. *Geochemistry International* **52**, 336–346 (2014).

30. Orvošová, M., Deininger, M. & Milovskỳ, R. Permafrost occurrence during the Last Permafrost Maximum in the W estern C arpathian M ountains of S lovakia as inferred from cryogenic cave carbonate. *Boreas* **43**, 750–758 (2014).

31. Bartolomé, M. *et al.* Characteristics of cryogenic calcites in Pyrenean ice caves of the Pyrenees (Northern Spain). *Geogaceta* 107–110 (2015).

32. Ramsey, C. B. Development of the radiocarbon calibration program Oxcal. *Radiocarbon* **43**, 355–363 (2006).

33. Munroe, J. S. First Investigation of Perennial Ice in Winter Wonderland Cave, Uinta Mountains, Utah, USA. *The Cryosphere Discussions* 1–31 (2020) doi:doi.org/10.5194/tc-2020-152.

34. Reimer, P. J. *et al.* The IntCal20 northern hemisphere radiocarbon age calibration curve (0–55 cal kBP). *Radiocarbon* **62**, 725–757 (2020).

35. Richter, D. K., Meyer, S., Scholz, D. & Immenhauser, A. Multiphase formation of Weichselian cryogenic calcites, Riesenberg Cave (Süntel/NW Germany)[Weichselzeitliche mehrphasige Genese kryogener Calcite in der Riesenberghöhle des Süntel (Weserbergland/NW Deutschland)]. *Zeitschrift der Deutschen Gesellschaft für Geowissenschaften* **164**, 353–367 (2013).

36. Colucci, R. R. *et al.* First alpine evidence of in situ coarse cryogenic cave carbonates (CCCcoarse). *Geografia Fisica e Dinamica Quaternaria* **40**, 53–59 (2017).

37. Lacelle, D., Lauriol, B. & Clark, I. D. Formation of seasonal ice bodies and associated cryogenic carbonates in Caverne de l'Ours, Québec, Canada: Kinetic isotope effects and pseudo-biogenic crystal structures. *Journal of Cave and Karst Studies* **71**, 48–62 (2009).

38. Bella, P. Morphology of ice surface in the Dobšiná Ice Cave. in *2 nd International Workshop on Ice Caves. Proceedings. Slovak Caves Administration, Liptovskỳ Mikuláš* 15–23 (2007).

39. Marshall, P. & Brown, M. C. Ice in Coulthard Cave, Alberta. *Canadian Journal of Earth Sciences* **11**, 510–518 (1974).

40. Vaks, A. *et al.* Speleothems reveal 500,000-year history of Siberian permafrost. *Science* 1228729 (2013).

41. Pielsticker, K. H. Höhlen und Permafrost–thermophysikalische Prozesse von Höhlenvereisungen während des Quartärs. *Bochumer Geol. Geotech. Arbeit* **55**, 187–196 (2000).

42. Kern, Z. & Perşoiu, A. Cave ice–the imminent loss of untapped mid-latitude cryospheric palaeoenvironmental archives. *Quaternary Science Reviews* **67**, 1–7 (2013).

43. Spötl, C. & Vennemann, T. W. Continuous-flow isotope ratio mass spectrometric analysis of carbonate minerals. *Rapid communications in mass spectrometry* **17**, 1004–1006 (2003).

44. Spötl, C. Long-term performance of the Gasbench isotope ratio mass spectrometry system for the stable isotope analysis of carbonate microsamples. *Rapid Communications in Mass Spectrometry* **25**, 1683–1685 (2011).

45. Burns, S. J. *et al.* Rapid human-induced landscape transformation in Madagascar at the end of the first millennium of the Common Era. *Quaternary Science Reviews* **134**, 92–99 (2016).
46. Jaffey, A. H., Flynn, K. F., Glendenin, L. E., Bentley, W. t & Essling, A. M. Precision measurement of half-lives and specific activities of U 235 and U 238. *Physical review C* **4**, 1889 (1971).
47. Edwards, R. L., Gallup, C. D. & Cheng, H. Uranium-series dating of marine and lacustrine carbonates. *Reviews in Mineralogy and Geochemistry* **52**, 363–405 (2003).
48. Cheng, H. *et al.* Improvements in 230 Th dating, 230 Th and 234 U half-life values, and U–Th isotopic measurements by multi-collector inductively coupled plasma mass spectrometry. *Earth and Planetary Science Letters* **371**, 82–91 (2013).

Figures

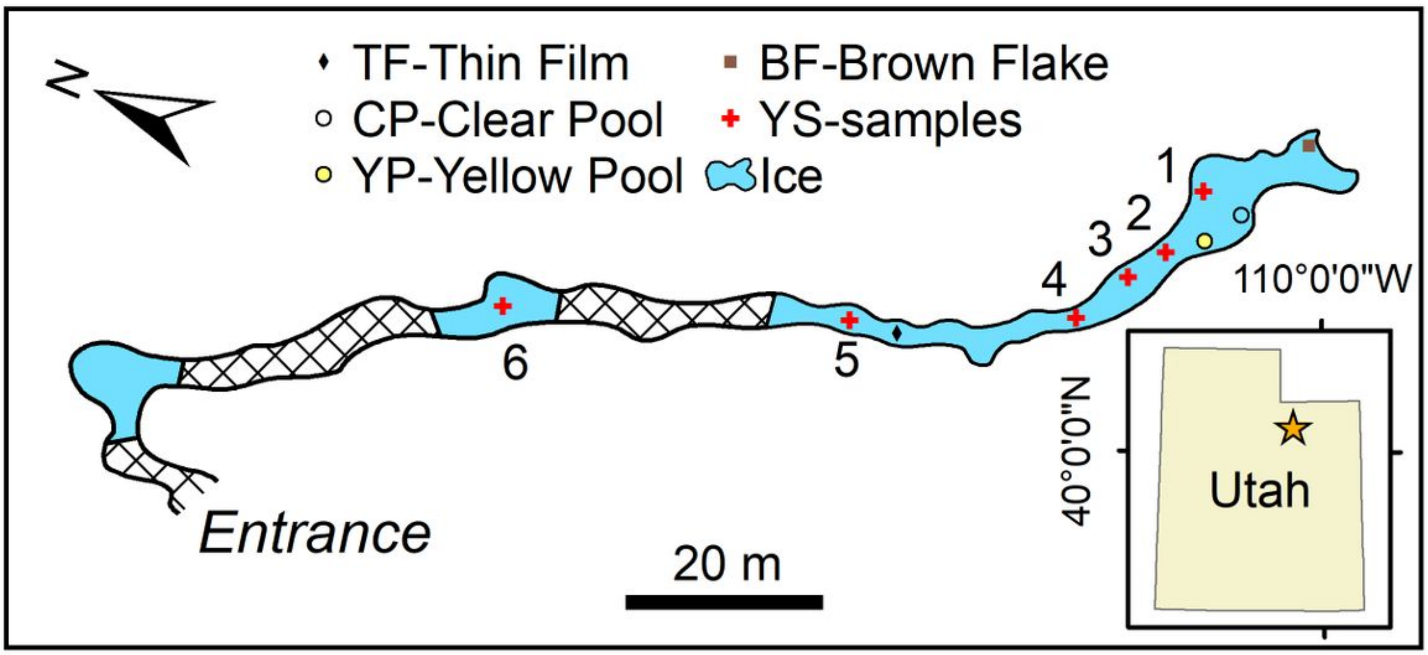

Figure 1

Map of Winter Wonderland Cave showing sections of the cave floored by ice (blue) and sampling locations. Inset shows the location of the cave in northeastern Utah (star).

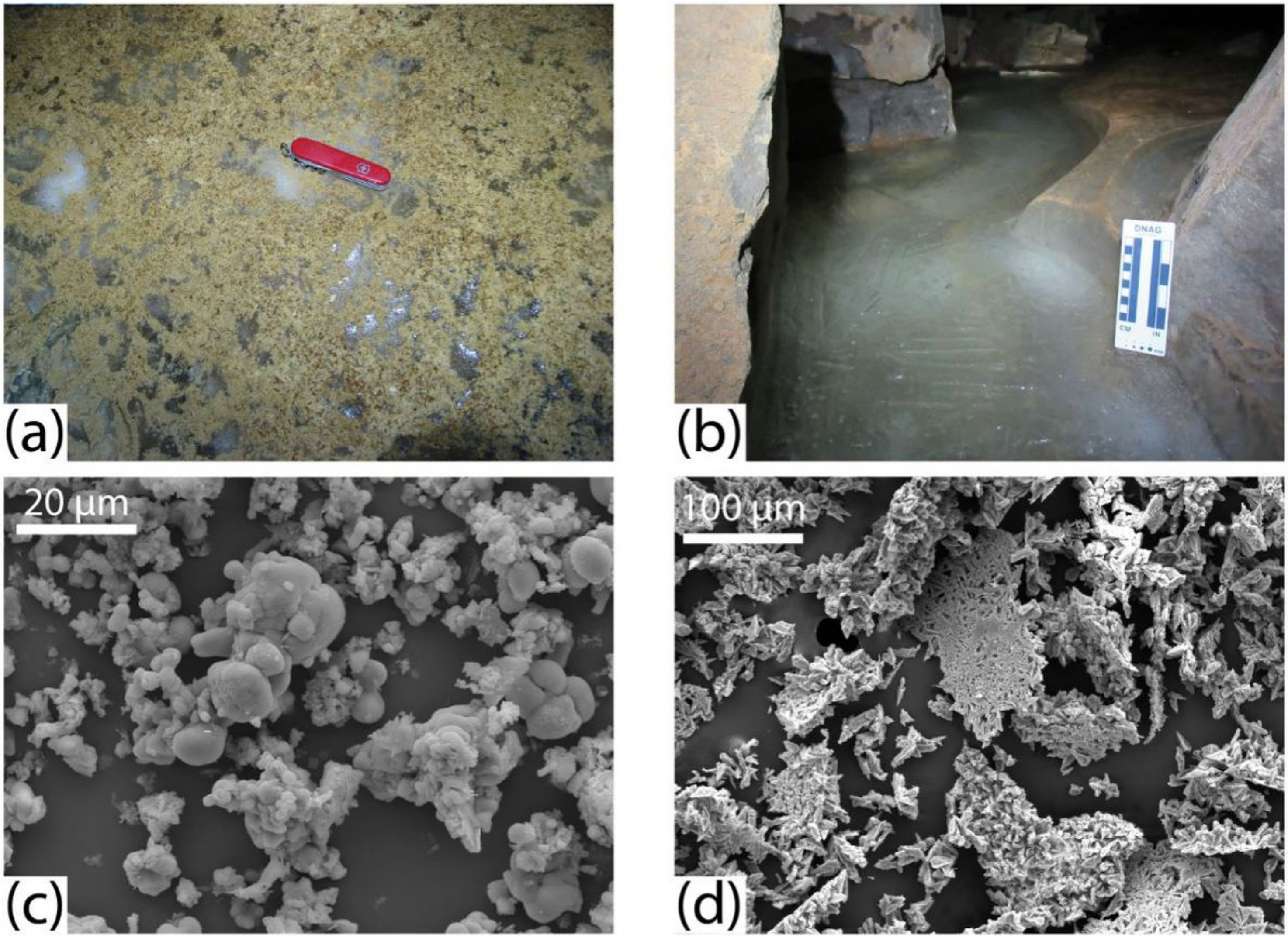

Figure 2

(a) Loose CCCcoarse on the surface of the ice. Red knife is 10 cm long. (b) Pool of water with a lid of ice along the edge of the perennial ice. (c) SEM image of sample YS-6 (CCCcoarse) at 2000× magnification showing calcite spherules. (d) SEM image of sample TF (CCCcoarse) at 500× magnification showing calcite rafts.

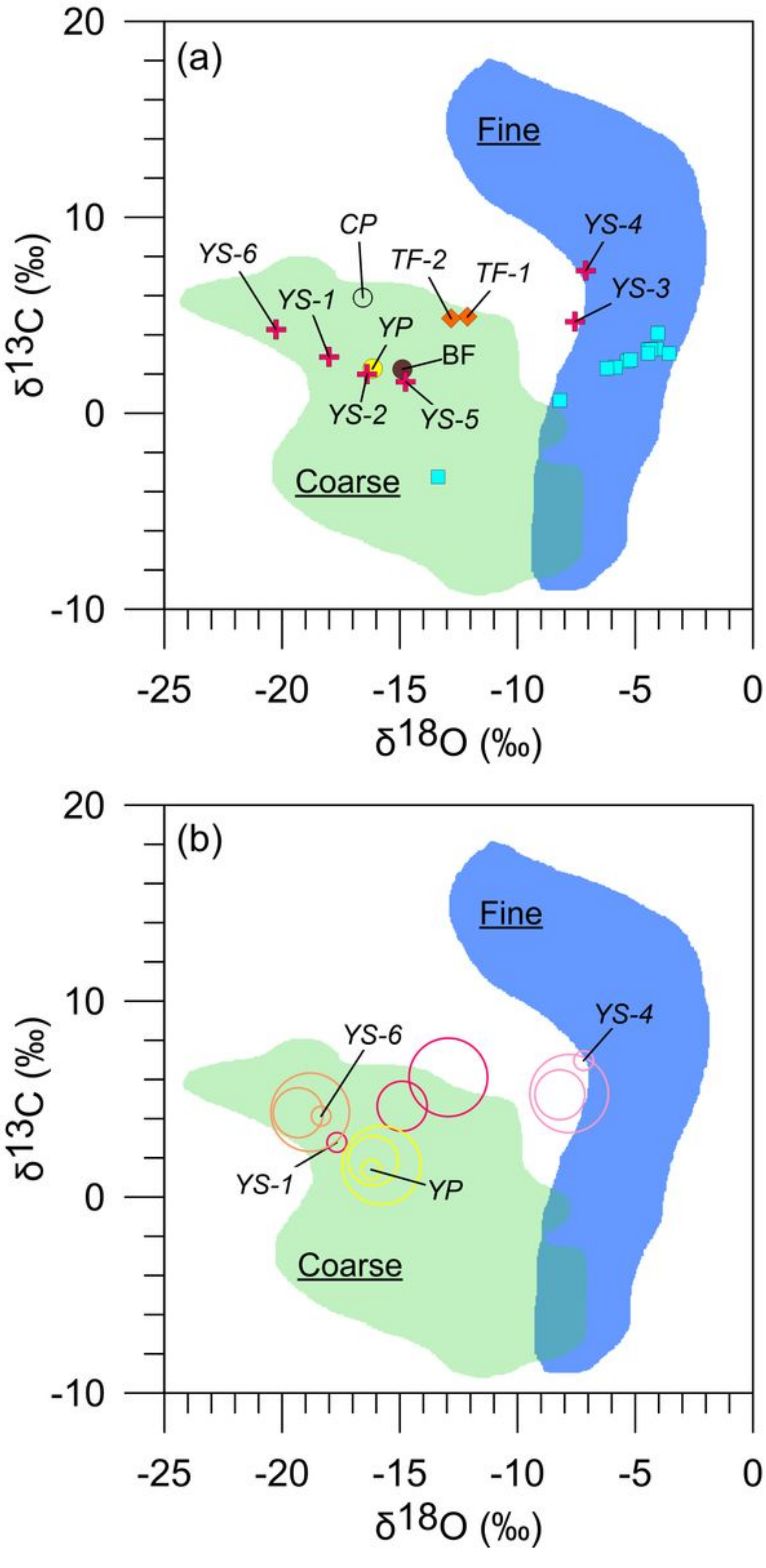

Figure 3

(a) Isotope data for samples from WWC: blue squares are bedrock; red crosses are CCC from the ice surface; CP and YP are CCC from the “clear” and the “yellow” pools, respectively; BF is from a layer of CCC within the perennial ice body. The blue and green polygons delineate the typical range of isotope values for CCCfine and CCCcoarse after 26. (b) Isotope values for samples YS-1, YS-4, YS-6, and YP presented by size fraction: large circle, 250-165 μm; medium circle, 165-75 μm; small circle, <75 μm.

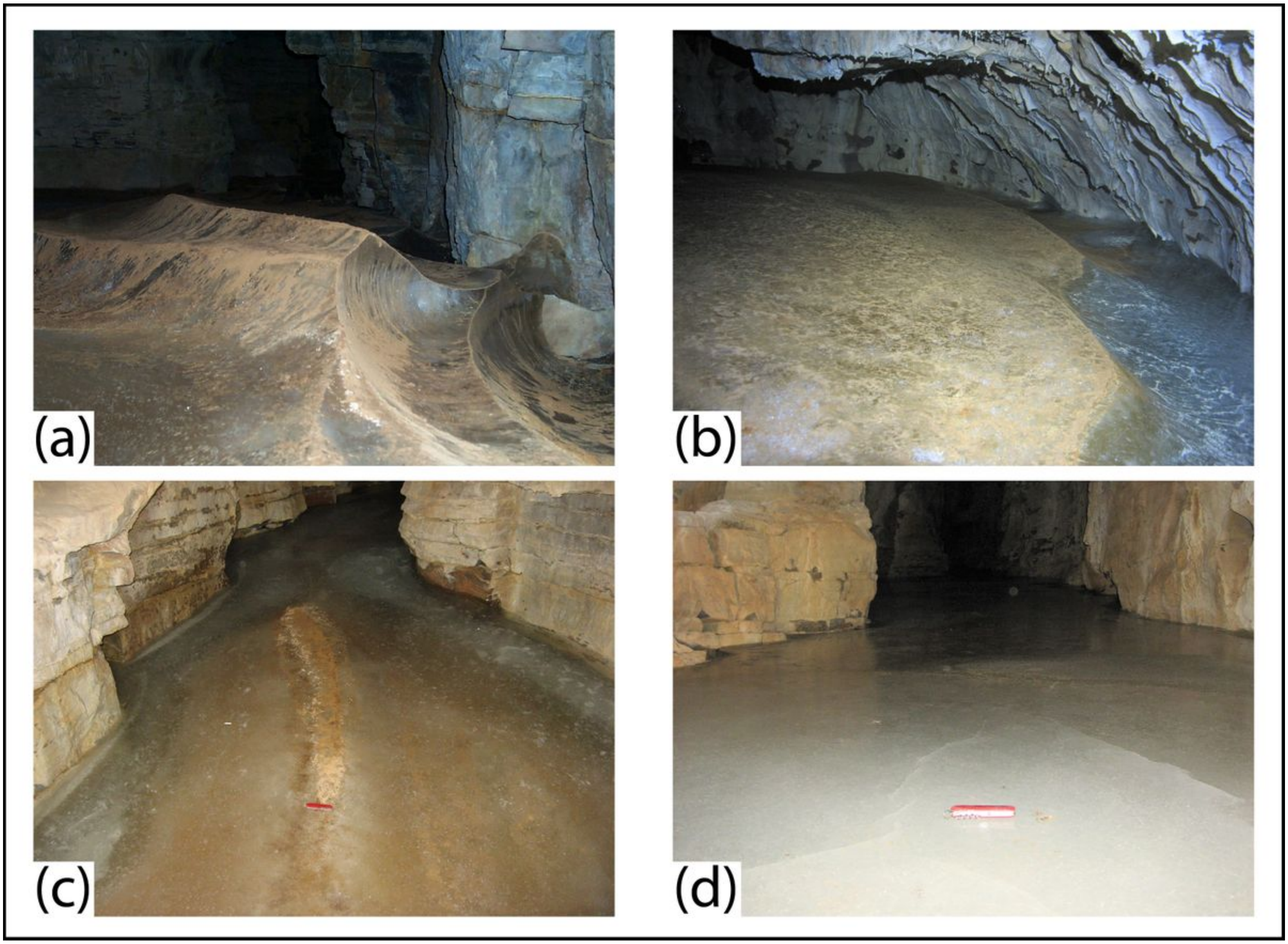

Figure 4

A selection of photographs highlighting recent changes observed in WWC. (a) The sculpted surface of the ice in 2016 illustrating intersecting cuspate forms produced by sublimating air currents. The total relief is ~30 cm. CCC is visible as tan material on the ice surface. (b) A view showing the edge of the ice in 2016 where a ~20-cm-deep moat had formed at the contact with the rock wall of the cave. (c) The surface of the ice in 2018 illustrating how inflowing water had submerged nearly all of the former sculpted surface beneath new ice. The red knife is located at the end of a ~1-m long section of a former crest in the ice that reaches barely above the new ice surface. (d) Another view from 2018 where new ice formed from inflowing water has completely inundated the former sculpted ice surface. Red knife is 10 cm long.

Supplementary Files

This is a list of supplementary files associated with this preprint. Click to download.

- SupplementaryInformation.pdf